Neuroscience 587 (2025) 146–156

Contents lists available at ScienceDirect

Neuroscience

journal homepage: www.elsevier.com/locate/nsc

Research Article

The Smarce1 subunit of the BAF complex performs distinct, stage-specific functions during zebrafish retinal development

Laura Ramírez [a], Denhí Schnabel [a], Flavio R. Zolessi [b,c], Hilda Lomelí [a,*]

[a] Departamento de Genética del Desarrollo y Fisiología Molecular. Instituto de Biotecnología, Universidad Nacional Autónoma de México, México
[b] Sección Biología Celular, Facultad de Ciencias, Universidad de la República, Uruguay
[c] Institut Pasteur de Montevideo, Uruguay

ARTICLE INFO

Keywords:
Chromatin remodeling
Smarce1
Retina
Zebrafish eye

ABSTRACT

In the developing vertebrate retina, progenitor cells proliferate and differentiate into specialized neurons with remarkable spatial and temporal precision. This process is coordinated by multiple interactions between the genome and the epigenome. Chromatin remodeling plays an important role in the regulation of retinal cell type-specific transcriptional programs. Vertebrate switch/sucrose non-fermentable (SWI/SNF) complexes, also known as Brg1/Brg-associated factors (BAF complexes) are multi-subunit, ATP-dependent chromatin-remodeling complexes assembled from homologous subunit families. The ATPase subunit of these complexes, Smarca4 (also known as Brg1), has been implicated in retinal development. Among the other core subunits, one that is incorporated early into the BAF complex is Smarce1 (also known as Baf57), which is present in all BAF assemblies. Notably, recent findings show that this protein acts as a mitotic bookmark in mouse embryonic stem cells to preserve cell identity during cell division.

In this work, we examined the retinal phenotype in *smarce1* zebrafish mutants and compared it with that in *smarca4* mouse and zebrafish mutants. The *smarce1* gene was differentially expressed in progenitors and neurons during development. We found that Smarce1 deficiency reduces the cell proliferation of retinal progenitors and produces a severe cell death. Although all classes of retinal neurons are specified in *smarce1* embryos, normal lamination of retinal cells is altered and differentiation of photoreceptors is deficient.

Given that not all of these phenotypes are observed in the zebrafish *smarca4/Brg1*-mutant, we propose that a differential configuration of the BAF complex in the retina contributes to distinct functions during retinogenesis.

Introduction

In vertebrates, the retina has a simple anatomical structure and a limited number of neuronal cell types. For this reason, it is one of the preferred model systems for the study of neurogenesis. It is composed of six types of neurons that are morphologically and functionally distinct, and a glia cell-type called Müller cell. The types of neurons in the retina are ganglion cells (RGCs), amacrine cells (ACs), bipolars cells (BPs), horizontal cells (HCs), and rod and cone photoreceptors (PRs). These retinal cell classes are located within three distinct nuclear layers and two synaptic plexiform layers (Norden, 2023; Niklaus and Neuhauss, 2017; Stenkamp, 2015). The function of the retina is to receive light and transduce it into membrane potentials that are transferred through the retinal interneurons until they reach the RGCs, whose axons form the optic nerve and transport the visual inputs to the brain.

In zebrafish, as in other vertebrates, the retina develops from multipotent retinal progenitor cells (RPCs). Differentiation starts with withdrawal of RPCs from the cell cycle, closely associated to cell-type commitment and cellular differentiation. All of the retinal cell types are derived from the same neuroepithelial RPCs, but the temporally conserved order in which cells leave the cell cycle determines their fate (Malicki et al., 2016). The first cells that leave the cell cycle are fated to become RGCs; successive waves generate cone cells, ACs and HCs. The late born cell types are rods, BPs and Müller glia (Norden, 2023; Niklaus and Neuhauss, 2017; Stenkamp, 2015).

The specific differentiation pathways undertaken by each cell type is coordinated by complex networks of transcription factors. RPC competence varies during development. Thus, RPCs have different capacities for the integration of signalling pathways as development progresses. Among the mechanisms that determine the changes in competence is

* Corresponding author.
E-mail address: hilda.lomeli@ibt.unam.mx (H. Lomelí).

https://doi.org/10.1016/j.neuroscience.2025.09.045
Received 5 July 2025; Accepted 29 September 2025
Available online 4 October 2025

chromatin regulation (Raeisossadati et al., 2021; Yin et al., 2023). Chromatin configurations in the RPCs, could lead to diverse interpretations of the same genome, leading to specific transcriptional outputs and the generation of different cell identities. A central mechanism for the control of DNA accessibility is the mobilization of nucleosomes which is mediated by chromatin remodelers. These are large multimeric protein complexes that break histone–nucleotide contacts through ATP hydrolysis (Gourisankar et al., 2024; Aigner et al., 2007). Chromatin remodelers are involved in multiple aspects of retinal development. Specifically, the SWI/SNF or BAF complex have been studied in this context (Kadoch and Crabtree, 2015; Hodges et al., 2016). BAF complexes are assemblies of approximately 16 subunits encoded by 29 genes. These complexes are polymorphic, as they are built from the combinatorial assembly of paralogous subunits (Hodges et al., 2016; Mashtalir et al., 2018). The diversity of complexes generated allows a functional multiplicity associated with specific lineages or cell types (Lessard et al., 2007).

BAF complexes open chromatin and recruit transcriptional regulators; thus, they play a central role in the regulation of gene expression. The catalytic subunits of BAF complexes are SMARCA4 and SMARCA2 (also known as BRG1 and BRM respectively), which encode ATPases (Kadoch and Crabtree, 2015). A mutation in the zebrafish *smarca4* gene was identified as the *young* mutation (Gregg et al., 2003; Link et al., 2000). Among other phenotypes, this mutation causes a severe malformation of the eye. In *young* mutants, the pattern of cell cycle withdrawal in the developing retina is normal and the specification of major cell types occurs, but retinal differentiation is inhibited, and retinal lamination is absent or severely disrupted. Smarca4 is an irreplaceable member of the BAF complex; thus, it is expected to be very sensitive to loss-of-function mutations, as in fact was demonstrated (Gourisankar et al., 2024). In contrast, accessory or paralogous subunits that can be substituted, are more tolerant to mutations. Nonetheless, some of these subunits, which might be responsible for specific interactions with transcription factors or be critical for DNA binding in particular regions of the genome, could be important for the specification of cell-type or developmental specific functions. In particular, for the development of retinal neurons, which depends on the distinct responses of RPCs, learning the contributions of accessory subunits to differential functions of the BAF complex during retina development is a relevant question.

SMARCE1 (or BAF57) is an animal-specific subunit that is present in all of the canonical BAF assemblies (Lomeli and Castillo-Robles, 2016). Although SMARCE1 lacks homologous genes, Kazantzeva *et al* reported that N-terminally truncated SMARCE1 isoforms produced by alternative splicing, are specifically expressed in the neurons of humans and rodents (Kazantseva et al., 2009). The main structural feature of SMARCE1 is a high-mobility-group (HMG) domain, which promotes binding to topologically restricted DNA in the form of a cruciform structure. SMARCE1 interacts with a wide range of protein partners outside the BAF complex. Recent work with mouse embryonic stem cells revealed individual interactions of Smarce1 and Smarcb1 with chromatin (Zhu et al., 2023). Unlike Smarca4, these subunits bind to promoters during mitosis. For Smarce1 they show that its binding to mitotic chromatin functions as a bookmark and is essential for the reactivation of gene expression after mitotic exit. In this study, the authors suggest that Smarce1 acts as an early assembly component of the BAF complex. Interestingly, Smarce1 deficiency caused the upregulation of neural differentiation genes.

In a previous study, we analyzed the phenotype of zebrafish with the loss-of-function *smarce1* gene mutation (Castillo-Robles et al., 2018). Similar to the *young* mutation, *smarce1* mutation caused microphthalmia, abnormal body curvature and severe heart abnormalities. In this work, we analyzed the phenotype in the retina of *smarce1* mutants in comparison with that of *young* mutants. We found that Smarce1 deficiency reduced the proliferation of retinal progenitors and resulted in severe cell death. Although all classes of retinal neurons are specified in *smarce1* embryos, normal organization of retinal cells is altered and the differentiation of photoreceptors is deficient. A comparison of this phenotype with that observed in fish and mice Smarca4 mutants suggested that Smarce1 performs distinct functions in the BAF complex during eye development.

Experimental procedures

Zebrafish maintenance and strains

Wild type zebrafish (*Danio rerio*), *smarce1* mutants and transgenic lines SoFa1 (Almeida et al., 2014; Zolessi et al., 2006) and *atoh7*:gapEGFP (Bernardos and Raymond, 2006), were housed in a recirculating water system under controlled conditions of 14 h light and 10 h dark at 28 °C. To obtain the double *smarce1*$^{-/-}$/SoFa embryos; crosses between heterozygotes *smarce1* mutants and SoFa were set. Fluorescent positive larvae were selected under the stereomicroscope, and genotyped for *smarce1* with primers flanking the mutated site as described in (Castillo-Robles et al., 2018). Heterozygous *smarce1*$^{-/+}$/SoFa were crossed to obtain homozygous *smarce1*$^{-/-}$/SoFa fish. Embryos were obtained from natural crosses; parental fish were bred for 20 min before embryo collection. Embryos were cultured in a Petri dish in an incubator at 28 °C until the desired stage was reached. The staging was performed according to the Kimmel system (Kimmel et al., 1995).

Zebrafish were handled according to local animal regulations and experiments were approved by the Institutés Ethical Committee (Biotechnology Institute, UNAM).

Histology

Larvae (5dpf) were fixed overnight at 4 °C in Bouin's solution. After washing with PBS, they were dehydrated through a series of graded ethanol and embedded with paraffin. Tissue sections of 10 µm were cut and stained in hematoxylin-eosin based on a reported protocol (Cardiff et al., 2014).

Immunofluorescence

Whole-mount immunofluorescence was performed with slight modifications as previously described (Mendieta-Serrano et al., 2019). Briefly, embryos were fixed overnight at 4 °C in PFA 4 %, larvae were grown in 0.003 % PTU and collected at 5 dpf, fixed overnight at 4 °C in PFA 4 %; washed in blocking solution (PBS1X, Triton 0.1 %, BSA 5 %) for 3 h and then, primary antibodies diluted (1:100) in blocking solution; embryos and larvae were incubated overnight at 4 °C SMARCE1 (Abcam ab131328), zpr1 (ZIRC) and p- Histone H3 (sc-374669, Santa Cruz). Subsequently, larvae were washed twice in blocking buffer and embryos were incubated with secondary antibodies either Alexa 647 (A21244, Invitrogen) or Alexa fluor 488 (A12379 Invitrogen) overnight at 4 °C. Larvae were washed 3 times with blocking solution and incubated for 3 h in methyl green (Prieto et al., 2015) or 1 h in DAPI for nuclear staining and mounted for confocal laser scanning microscopy in 75 % glycerol, 0.1 M Tris·HCl pH 8 as previously described.

Immunofluorescence on cryostat sections was performed as previously described (Letelier et al., 2023). Embryos were fixed by immersion in 4 % PFA at 4 °C overnight. Then, embryos were incubated in 30 % sucrose overnight at 4 °C and processed for embedding frozen tissue in OCT compound (Tissue Tek, Miles Scientific, MA, USA). Transverse sections of 20-µm-thick were cut using a cryotome and stored at −70 °C until processing. Immunostaining of phospho-histone 3 was performed using p-Histone H3 (sc-8656, Santa Cruz) primary antibody and secondary goat anti rabbit Alexa 488 (A12379 Invitrogen).

Confocal laser scanning microscopy and image analysis

Larvae from the different treatments were anesthetized using tricaine (Sigma) and mounted in 0.5 % low-melting point agarose in order to be imaged by fluorescent microscopy using either Zeiss spinning disk

or the Confocal Olympus FV1000 Inverted with 40X and 60X objectives. Samples were excited with 405 nm, 488 nm or 635 nm light depending on the fluorescent dye used. Image acquisition was performed with the same gain amplification and exposure times to be able to compare experimental conditions with the corresponding controls. Image stacks were merged into a single focused image with Fiji software.

Quantification of proliferation and cell death

For quantitative analysis of cell death at 72 hpf and 5 dpf pyknotic nuclei were stained with methyl green. Between 8 and 11 larvae were imaged per condition. The numbers of nuclei with enhanced fluorescence (pyknotic nuclei) were manually counted from Z-stack confocal images.

To quantify cell proliferation at 5 dpf, pH3 + cells in the CMZ were manually counted from confocal images of 7 to 9 sections encompassing the central region of the retina. Ten retinas were imaged per condition. For each eye, the average number of pH3 + cells per section was calculated, and the total number of pH3 + cells per retina was also reported. For quantification at 48 hpf, genotypes were determined by PCR described in Castillo *et al* (Castillo-Robles et al., 2018). The number of PH3 cells was then counted in sections containing the central retina, recognized by the presence of the optic nerve and the largest lens diameter. Total mitotic counts were normalized to retinal area (mm^2). In addition, PH3 + cells within the ONL were quantified and normalized to the corresponding retinal area. Six control and five mutant retinas were analyzed.

For statistical analysis, data distribution was assessed using the Shapiro–Wilk test. Comparisons between two independent groups were performed using Student *t*-test (equal variances) or Welch's *t*-test (unequal variances) and non-parametric data were analysed using the Mann-Whitney U tests. Apoptotic and proliferative cells were quantified using Fiji software and statistical analyses were performed with Prism 6 (GraphPad Software, La Jolla, CA, USA).

RNA-sequencing and data analysis

Pools of 60 dissociated eyes from 5dpf larvae (WT and *Smarce1*$^{-/-}$) of three independent crosses were used for RNA extraction (Zymo Research). Each RNA sample was analyzed for quantity and purity with an Agilent 2100 Bioanalyzer (Agilent Technologies, CA, USA). Libraries and RNA sequencing and data analysis were conducted under contract by Novogene Co., Ltd according to their protocols, sequencing libraries were generated NEBNext®Ultra™RNA Library Prep Kit for Illumina® (NEB, USA) following manufacturers' recommendations and index codes were added to attribute sequences to each sample. Library preparations were sequenced on an Illumina platform and 125 bp/150 bp paired-end reads were generated. Raw reads were filtered and aligned with reference genes. The alignment data was utilized to calculate the distribution of reads on reference genes and the mapping ratio. The fragments per kilobase of transcript per million mapped reads (FPKM) method was used to calculate the expression levels. Differential expression analysis between two groups (≥three biological replicates per condition) was performed using the DESeq2 R package (1.14.1). The resulting P-values were adjusted using Benjamini and Hochberg's approach for controlling the False Discovery Rate (FDR). Genes with an adjusted P-value < 0.05 found by DESeq2 were assigned as differentially expressed. Gene Ontology (GO) enrichment analysis of differentially expressed genes was determined with the clusterProfiler R package. GO terms with a P-value less than 0.05 were considered significantly enriched. Kyoto Encyclopedia of Genes and Genomes (KEGG) pathway enrichment was performed for the analysis of gene functions to obtain information on the cellular process of differentially expressed genes.

Results

Retinal progenitors of Smarce1 mutants have a reduced cell proliferation

In a former study we generated two CRISPR/Cas9 mutant alleles with four-and eight-nucleotide deletions in exon 4 of the *smarce1* gene. Both alleles exhibited morphological defects detectable on day 3 (dpf), which included a curvature of the tail, reduced eye size and swelling of the pericardium. In that study we focused on the function of Smarce1 in heart development (Castillo-Robles et al., 2018). Posterior transcriptomic analysis of whole 5 dpf mutant embryos revealed that phototransduction was among the most affected pathways. In this work we carried out an analysis of eye development in the 8-base pair deletion allele. We used an anti-Smarce1 antibody for immunodetection in the retina. At 30 hpf, we detected a Smarce1-positive signal in nuclei of all RPCs (Fig. 1A). Later, at 5 dpf, we found the strongest signal of Smarce1 in a group of ACs of the inner nuclear layer and in very few, scarce, RGCs. Smarce1 immunostaining in *gfap*-GFP transgenic retinas confirmed that the signal did not overlap with the soma of Müller glia cells (data not shown). The signal was also detected in the Photoreceptor layer (PL) (Fig. 1A).

Histological analysis of the *smarce1* mutant retinas confirmed the reduction in eye size, which ranged from 70 to 50 % of the normal size, depending on the phenotype penetrance. Also depending on the penetrance, some retinas showed a complete loss of lamination and absence of plexiform layers (Fig. 1B). In less severe cases, the layers were visible (Fig. 2), but neurons were mislocalized, and the plexiform layers appeared thinner or irregular. To analyze if the retinas of *smarce1* homozygous mutants had a reduced proliferation we performed immunofluorescence using a primary antibody specific for the phosphorylated form of histone H3 (PH3) at serine 10. In cryostat sections of 10 control 5 dpf embryos we detected the mitosis of RPCs in the ciliary margin zone (CMZ). In contrast, in sections of 10 *smarce1*-mutants, we identified mitotic RPCs only very rarely (Fig. 2A). Quantification of the mitotic cells revealed a significant reduction in the abundance of these cells in the mutants (Fig. 2B). To determine whether mitosis of undifferentiated proliferating cells at earlier stages is also affected in the *smarce1*-mutants, we quantified cell proliferation in 48 hpf retinas. At this stage, cell proliferation is still considerable; accordingly, cryostat sections showed numerous mitotic cells across different retinal layers, with the highest numbers in the outer nuclear layer, corresponding to the PR lineage (Supplementary Fig. 1A). After quantification of six control and five mutant retinas, we found a tendency toward fewer PH3-positive cells in the *smarce1*-mutant retinas; however, the difference between control and mutant samples was not statistically significant (Supplementary Fig. 1B). These results suggest that the reduction in cell proliferation primarily affects CMZ cells.

Transcriptomic analysis of smarce1-mutant retinas confirmed the downregulation of cell cycle-related genes

We proceeded to obtain transcriptomes from dissected eyes of 5 dpf *smarce1*-mutant and wild-type embryos. Pearson correlation coefficient analysis and principal component analysis revealed clustering of the three mutant and three wild-type biological replicates of each population, demonstrating that the two embryo groups were highly distinct (Supplementary Fig. 2). Differential expression analysis uncovered 4399 differentially expressed genes (DEGs), of which 2114 were downregulated and 2285 were upregulated in the mutants.

Initially, for the analysis of the DEGs we used the gene sets identified by Xu *et al* in a single-cell transcriptomic study (Xu et al., 2020). In this work they identified seven distinct developmental states characterized by specific markers through single-cell RNA sequencing of the zebrafish retina at 24, 36, and 48 hpf and 14 dpf. A comparison of their clusters with our downregulated DEGs revealed that among the overlapping genes, the most abundant in the *smarce1*-mutant retinas belonged to

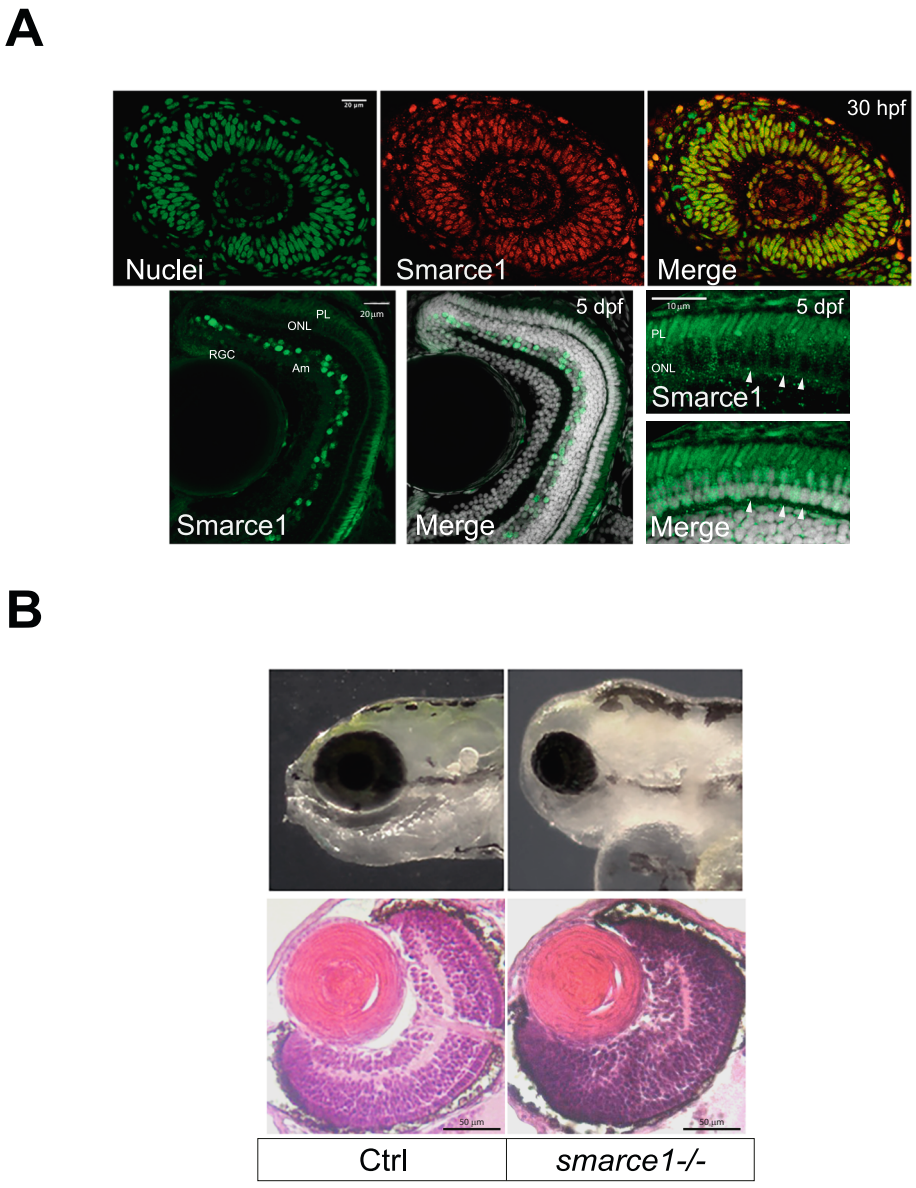

Fig. 1. Immunodetection of Smarce1 in retinas at 30 hpf and 5 dpf. (A) Confocal sections of a 30 hpf retina stained with a Smarce1 antibody (green) (upper panel); the signal is detected in all RPCs nuclei. Cryostat histological sections of 5 dpf retinas showing DAPI stained nuclei (gray) and Smarce1 signal (green) in amacrine cells (Am), retinal ganglion cells (RGC), Photoreceptor layer (PL), and outer nuclear layer (ONL) (lower panel). The high magnification images on the right show Smarce1 signal in most photoreceptor nuclei, except for a few basally-localized ones, which appear negative (arrowheads). Signal in outer segments (PL) is due to autofluorescence. (B) Bright-field photographs of wild type (Ctrl) and mutant (*smarce1*$^{-/-}$) heads showing the eye size reduction (upper panel). H&E sections of 5 dpf wild type (Ctrl) and mutant (*smarce1*$^{-/-}$) retinas (lower panel). Scale bars in A: 20 µm; in B: 50 µm. (For interpretation of the references to colour in this figure legend, the reader is referred to the web version of this article.)

clusters 1 (118) and 2 (73) of their study (Supplementary Table 1). These genes represent progenitor cells and rapidly proliferating RPCs, the disruption of which affects early retinal development. Among the most downregulated genes was *fabp11a* (fold change: 11.5, Padj: 1.66E-29), a gene whose knockdown causes a small eye phenotype (Qi et al., 2016). Another gene whose expression was strongly reduced is *enhancer of zeste 2* (*ezh2)* (fold change: 4, Padj: 6.78E-37). The encoded protein is a core component of the polycomb complex PRC2, which promotes transcriptional silencing through the methylation of lysine 27 in histone H3 (H3K27me3). PRC2 is essential for the maintenance of retinal progenitor cells in mice, as it has been shown that *Ezh2*-deficient retinas exhibit cell proliferation defects and increased cell death, a phenotype similar to that described here (Iida et al., 2015; Zhang et al., 2015).

In this same study Xu *et al.* found the enrichment of cell cycle S/G2/M−related genes in the transition between two sequential distinct developmental states. The genes of these transitional clusters were severely downregulated (Fig. 3A) in *smarce1*-mutant retinas. Additionally, GO enrichment analysis confirmed that among the most significant term of the BP subclass was the cell cycle process, and accordingly, KEGG analysis revealed that the cell cycle pathway was the second most affected term in the *smarce1*-mutants (Fig. 3B, D). The other highly significant group of genes whose expression was downregulated was those related to DNA replication. In both the GO and KEGG analyses, this pathway appeared at the top of the lists. Specifically, *pcna* was the fifth most likely downregulated gene (fold change: 5.7, Padj: 1.53E-60). These results and the elevated number of downregulated RPC genes are in line with the reduced proliferation observed in the mutant retinas and suggest that the transition between different developmental states might be compromised in the *smarce1* mutants.

Another interesting result that emerged from the GO analysis is that

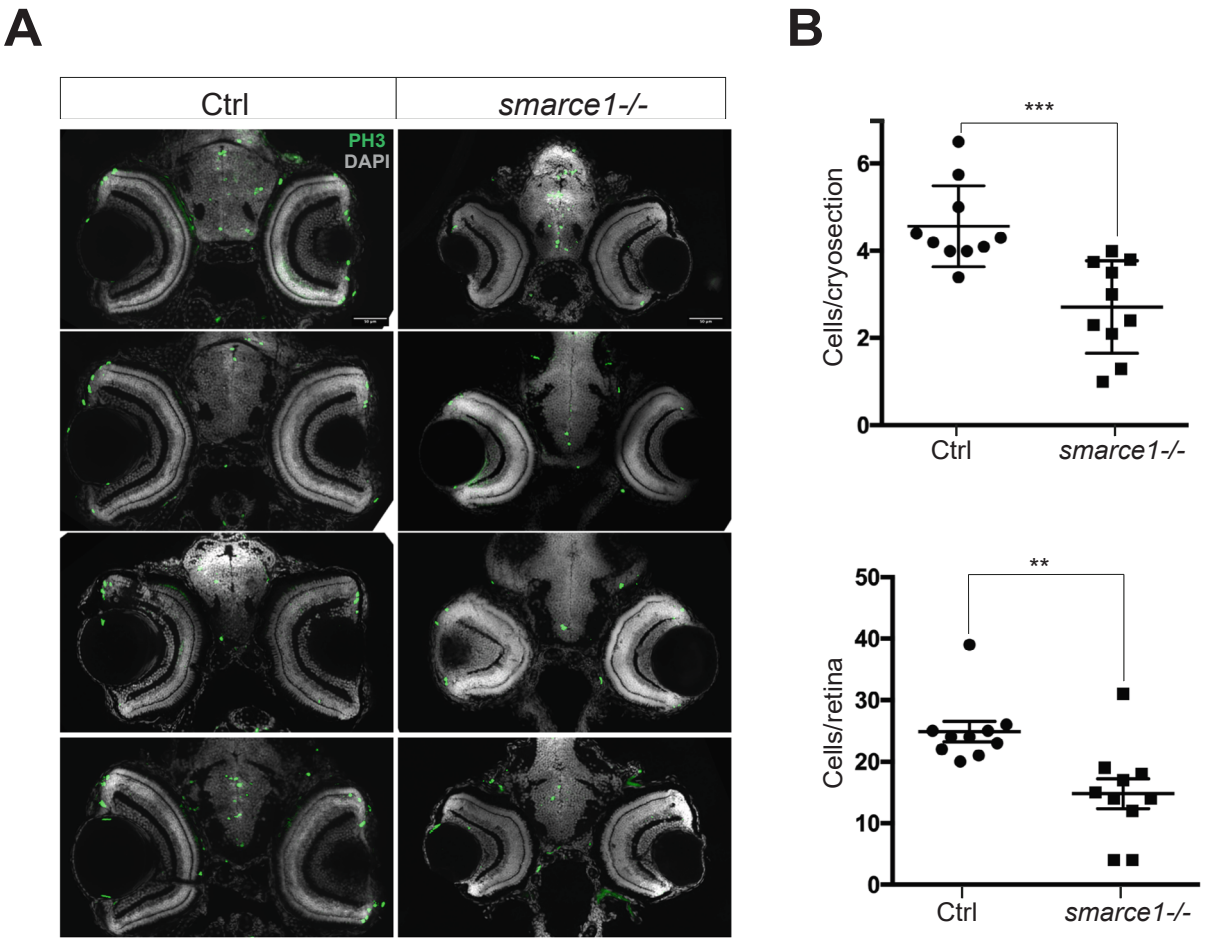

Fig. 2. Mitosis of RPCs in the CMZ of 5 dpf retinas. (A) Immunostaining with phospho-histone H3 (PH3) reveals mitotic cells in central retinal cryosections from wild-type (Ctrl) and mutant (*smarce1*$^{-/-}$) samples at 5 dpf. DAPI staining labels nuclei. A reduced number of PH3-positive cells is observed in *smarce1*$^{-/-}$ retinas compared to Ctrl. Scale bar: 50 μm. (B) Quantification of PH3 positive cells in WT and *smarce1*$^{-/-}$ retinas. The upper graph shows the average number of PH3 cells per section (7–10 sections); each dot represents one retina. For both control and *smarce1*$^{-/-}$ mutants, n = 10. The lower graph shows the total number of PH3-positive cells per retina. A significant reduction in PH3-positive cells was observed in *smarce*$^{-/-}$ samples compared to Ctrl (cells per section: $t_{18} = 4.14$, ***p = 0.0006; in total cells U = 9 **p = 0.002).

the top downregulated gene sets were specific to mitosis (for example, mitotic nuclear division, chromosome segregation, chromosome condensation, kinetochore and centromeric regions, and mitotic assembly) (Fig. 3E). These terms are relevant both in the context of the reduced detection of mitotic cells and in relation to the discovered bookmarking role of Smarce1 during mitosis in mouse embryonic stem (ES) cells, where similar gene sets were identified as binding sites for Smarce1 in mitotic chromosomes (Zhu et al., 2023). To evaluate whether Smarce1 could be involved in bookmarking in zebrafish, we performed subcellular Smarce1 detection in early zebrafish embryos. We used embryos at the oblong stage (3.7 hpf), where cells at different mitotic stages can be easily recognized. We found that Smarce1 was present in the nuclei of cells in the S-phase and early mitosis, but was clearly evicted from chromatin in telophase (Fig. 3C). This exclusion was also observed in 30 hpf retinas, where Smarce1 signal was absent in PH3-positive cells (Supplementary fig3A). These results indicate that in zebrafish, Smarce1 does not bookmark the nuclei of early embryos or retina progenitor cells *in vivo*.

Taken together, the results of PH3 detection and the transcriptomic analysis of the *smarce1*-mutant retinas indicate that the cell cycle is affected in both the S and the M phases.

Retinal neurons of the smarce1-mutants exhibited cell death

To analyze whether cell death contributes to the reduction in eye size, we used methyl green as a histological stain for DNA in fixed embryos (Prieto et al., 2015). Fluorescent nuclear labeling with this dye allowed the identification of dead cells in the retina. While control embryos did not show significant cell death at 3 or 5 dpf, we detected abundant cell death in the retinas of mutant embryos at these time points (Fig. 4A and Supplementary Fig. 3B). The quantification of pyknotic nuclei indicated that cell death was more common at 5 dpf than at 3 dpf (Fig. 4B,D). In addition, a quantification of cell death per layer revealed that cell death was more concentrated in the inner nuclear layer where AC, BC, Müller and HC cells reside, with ostensibly greater presence in the BC/Müller cell region (Fig. 4C,E). Increased cell death was accompanied by the upregulation of apoptosis-related genes, as indicated by the transcriptomic analysis, where apoptosis was revealed as one of the most upregulated gene pathways in *smarce1*-mutants (Fig. 4F,G).

The neuronal cell types of the retina were specified, but their organization was disrupted

Analysis of DEGs associated with neuronal differentiation indicated that early markers for the major neuronal types and Müller glia cells, such as *atoh7, vsx2, otx2b, ube2a, crx,* and *gfap,* were not among the differentially expressed genes, which indicates a correct cell fate commitment. Moreover, comparison with the genes identified in differentiated neurons in the single-cell study by Xu *et al*, revealed that

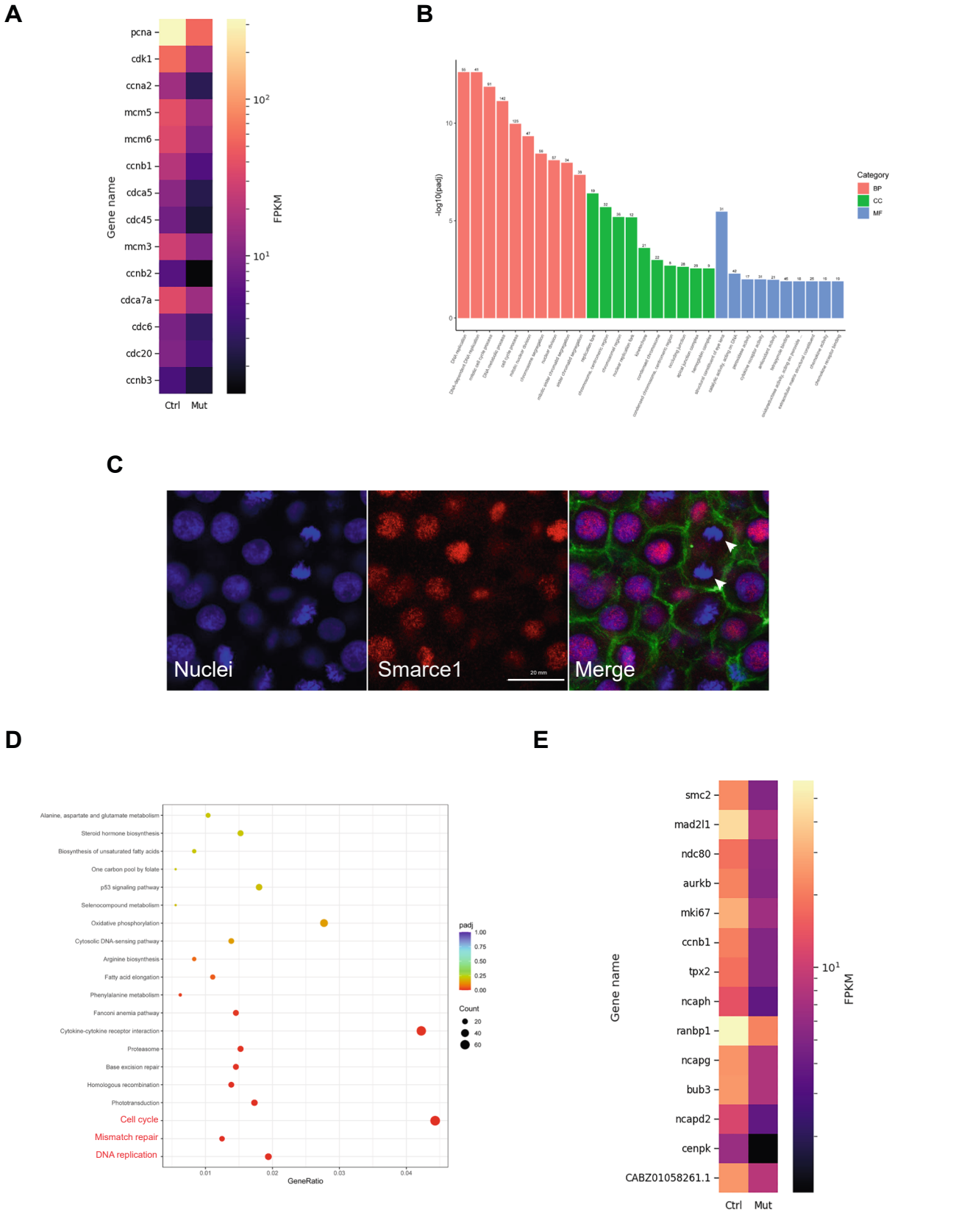

(caption on next page)

Fig. 3. Transcriptomic analysis of *smarce1*-mutant retinas confirms downregulation of cell cycle and mitosis genes. (A) Heatmap showing a list of the top downregulated genes of the Cell Cycle Term. The color bar shows the average FPKM value of three replicates. Yellow color indicates a high expression level, and black color indicates a low expression level. Genes are organized according to their Padj value from small to large (range 1.53e-57 to 3.7e-08). (B) GO enrichment analysis. The most significant 30 Terms were selected for display; the x-axis indicates GO Term, and the y-axis displays GO Term's level of significance of enrichment, expressed as −log10 (padj). Different colors represent different functional categories; BP: biological processes, CC: cell components, MF: molecular function. (C) Confocal images showing immunodetection of Smarce1 in embryos at the oblong stage (3.7 hpf). DAPI staining (blue) labels nuclei in S-phase and chromosomes at mitosis. Phalloidin (green) marks the cell cortex. Smarce1 signal (red) is localized to nuclei but is absent from mitotic chromosomes. Late anaphase/early telophase chromosomes in a dividing cell are indicated (white arrow heads). Scale bar: 20 μm. (D) KEGG enrichment results showing that the top downregulated pathways are related to the cell cycle (red characters); the most significant 20 KEGG downregulated pathways are displayed. The x-axis represents the ratio of the number of differential genes linked with the KEGG pathway to the total number of differential genes; the y-axis lists the KEGG pathways. The size of a point represents the number of genes annotated to a specific KEGG pathway. The color from red to purple represents the significant level of enrichment. (E) Heatmap showing the top downregulated genes of the Mitosis Term. The bar shows the average FPKM value of three replicates. Yellow color indicates a high expression level, and black color indicates a low expression level. Genes are organized according to their Padj value from small to large (range 1.32e-36 to 3.3e-18). (For interpretation of the references to colour in this figure legend, the reader is referred to the web version of this article.)

only a few genes in these cell clusters were differentially expressed in *smarce1* mutants, with the exception of phototransduction genes (Fig. 6A). Despite these molecular results, histological analysis revealed lamination defects. Then, for a detailed analysis of specific neuronal types, we applied fluorescent gene expression and antibody detection in 5 dpf embryos. *atoh7*:gapEGFP fish were used for the detection of RGCs (Bernardos and Raymond, 2006). Notably, the intensity of fluorescence was much weaker in the mutant retinas than in the wild-type retinas, which could indicate fewer RGCs. This was clearly appreciated in images of the optic nerve, along with disorganization of axons (Supplementary Fig. 4). Confocal images showed that RGCs in control embryos formed a compact basal layer adjacent to a correctly organized inner plexiform layer (IPL). In contrast, in the mutant retina, RGCs seemed less abundant and formed a thinner and very disorganized layer. These cells also had fewer axonic projections, suggesting a defective axonogenic process (Fig. 5). In the *atoh7*:gapEGFP mutant retinas, more fluorescent cells were detected in the outer regions. This could be the result of the retention of RGCs in the apical and midretinal positions, which would indicate a defective translocation process.

To examine AC and HC cells, we used *ptf1*a:EGFP SoFa fish (Zolessi et al., 2006). Images of 5 dpf mutant retinas revealed that the horizontal cell layer was not properly organized. The cells in this region had a rounded appearance and no connections established among them, which affected the formation of the outer plexiform layer (Fig. 5). Additionally, GFP-positive cells were mislocalized at a position where BCs reside, which suggests that the apical migration of HCs is delayed. ACs formed a layer that seemed normal, although with a reduced cellular density. In this regard, our RNAseq data indicated the downregulation of *ptf1a* (fold change: 2. 7, Padj: 2.9E-4), which could be indicative of a reduction in this cell population. Here, again, deficient IPL formation is evident.

In the case of PRs, both cone and rod markers associated with phototransduction and terminal differentiation were downregulated (Fig. 6A). To observe these cells in the retinas we used an antibody against Zpr1, a marker of double cone photoreceptors (Larison and Bremiller, 1990). In *smarce1* mutants, at 3 and 5 dpf, the majority of the cones were detected in their correct position of the distal retina; however, at both stages, a significant number of *zpr1*-positive cells were also observed in inner positions, mostly corresponding to the RGC layer. Cones located in the correct layer were elongated as normal photoreceptors, but when the whole row of cones was compared with the wild type pattern, disorganization was clearly appreciated, indicating that the layer was not correctly assembled (Fig. 6B).

Differential expression of nonneuronal markers

Other genes whose expression was downregulated in the *smarce1*-mutants were those of the lens. GO analysis of the MF subclass identified the structural constituents of the eye lens as the most significantly downregulated group (Fig. 3B). This group includes the majority of the crystallin proteins (Supplementary Fig. 5A). Bright field images of the lens in *smarce1*-mutant eyes showed a strong opacity, suggesting defective lens formation (Supplementary Fig. 5B).

Although we found a similar number of downregulated (2114) and upregulated (2285) genes in the *smarce1*-mutant eyes (Supplementary Fig. 1D), the majority of the upregulated genes were unrelated to eye development (Supplementary Table 1). Notably, all twenty of the top GO terms in the BP category were related to the immune response (Supplementary Table 1 and Supplementary Fig. 6). The implication of this result remains unclear. It is possible that these genes reflect an intense inflammatory response due to cell death, aberrant morphogenesis and retinal degeneration.

Discussion

In this work we have studied the role of the BAF subunit Smarce1 during the formation of the retina. The importance of comparing the functions of independent subunits of the BAF complex relies on the fact that this complex assembles different subunits in a combinatorial manner, with each subunit relating to a specific activity. The assemblies of the SWI/SNF family are classified into two main functionally distinct complexes according to their subunit compositions: BAF (with BAF250) and pBAF (with BAF180). In addition, there is a noncanonical combination (ncBAF) characterized by the presence of BRD9 (Gourisankar et al., 2024). SMARCE1 is interesting because it has no homologs and thus is present in all the combinations of the canonical BAF (cBAF) complexes, being absent only in ncBAF. Additionally, SMARCE1 has special functions both within and independent of the BAF complex, such as its mitotic bookmarking role in mouse embryonic stem cells and its role in stabilizing of the BAF180 subunit in the pBAF complex (Hah et al., 2010).

We found that the Smarce1 subunit was differentially expressed in specific regions of the retina. The neurons showing the most intense signal at 5 dpf were ACs, and with less intensity the RPCs, few RGCs and PRs. The high expression of *smarce1* in amacrine cells coincides with the results of the single-cell study reported by Xu *et al*, in which *smarce1* was listed among the genes expressed in cluster 4, which included ACs. The finding of an asymmetrical expression of Smarce1 in the retina was not obvious since Smarce1 assembles early in both cBAF complexes. This result suggests that most of the neuronal types do not contain any combination of cBAF complexes, although they could bear ncBAF assemblies. Also, it is possible that reduced amounts of Smarce1 are present in other cells of the retina, but were undetectable by our anti-Smarce1 antibody. At present, there is no available information regarding the subunit organization of the BAF complex in specific neuronal types of the retina in any animal model. This type of study would be helpful for elucidating the tissue-specific roles of remodeler assemblies.

Inactivation of Smarce1 in the zebrafish retina leads to a reduced size of the eyes and retina, likely caused by a combination of decreased progenitor cell proliferation and increased cell death during retinogenesis. We detected a reduction of cell proliferation by PH3 detection of mitotic cells in the CMZ of 5 dpf retinas. Although we did not perform

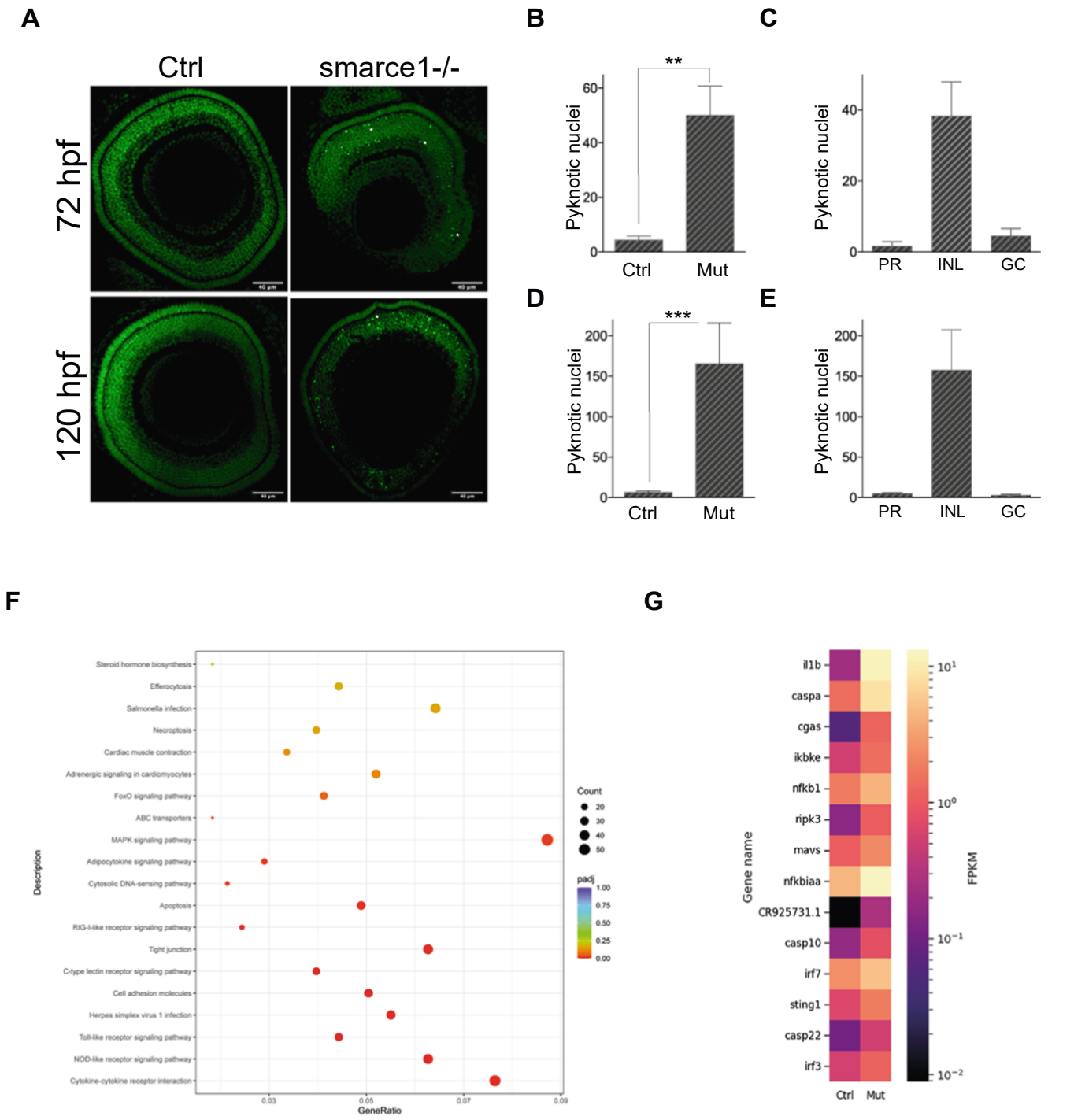

Fig. 4. Cell death of retinal neurons in the *smarce1*-mutants. (A) Confocal sections of 72 hpf and 5 dpf retinas stained with methyl green. Pyknotic nuclei representing apoptotic cells exhibit enhanced fluorescence (examples marked with an asterisk). Scale bar: 40 μm. (B and D). Quantification of the total number of pyknotic nuclei in WT (Ctrl) and *smarce1*$^{-/-}$ (Mut) retinas at 72 hpf (B) and 5 dpf (D). At 72 hpf, n = 8 for both, control and *smarce1*$^{-/-}$ mutants; at 5 dpf, n = 8 for control and n = 11 for mutant retinas. A Welchs *t*-test was performed showing a significant increase in pyknotic nuclei in *smarce*$^{-/-}$ samples compared to Ctrl. At 72 hpf ($t_6 = 4.11$, p** = 0.0058); at 5 dpf (U = 0,*** p = 0.0004). (C and E). Quantification of the number of pyknotic nuclei per layer in the *smarce1*$^{-/-}$ retinas at 72 hpf (C) and 5 dpf (E). PR: photoreceptors, INL: inner nuclear layer, GC, ganglion cell layer. (F) KEGG enrichment results show the upregulation of the apoptosis pathway (red), the most significant 20 KEGG upregulated pathways were selected for display. The x-axis represents the ratio of the number of differential genes linked with the KEGG pathway to the total number of differential genes; the y-axis lists the KEGG pathway. The size of a point represents the number of genes annotated to a specific KEGG pathway. The color from red to purple represents the significant level of enrichment. (G) Heatmap showing the top upregulated genes of the Apoptosis Term. The bar shows the average FPKM value of three replicates. Yellow color indicates a high expression level, and black color indicates a low expression level. Genes are organized according to their Padj value from small to large (range 1.72e-93 to 0.021). (For interpretation of the references to colour in this figure legend, the reader is referred to the web version of this article.)

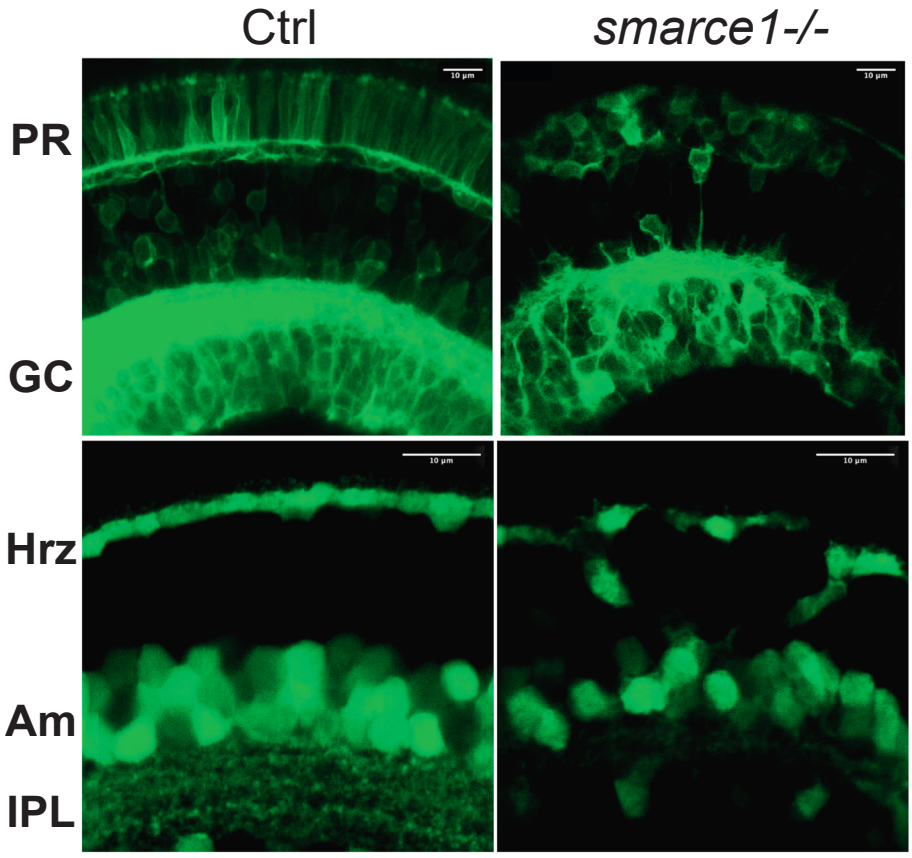

Fig. 5. Defective organization of ganglion, amacrine, and horizontal neurons. Confocal sections of 5 dpf Ctrl and *smarce1*$^{-/-}$ retinas expressing the ganglion cell reporter *atoh7*:gapGFP (upper panel) and *ptf1a*:cytGFP (lower panel). GC, ganglion cells; PR, photoreceptors; Hrz, horizontal cells; Am, amacrine cells; IPL, inner plexiform layer. Scale bars 10 µm.

any measurements in the S-phase, analysis of differential gene expression indicated that in addition to genes related to mitosis and the cell cycle, genes related to DNA replication were severely downregulated. Therefore, it is likely that both the S and M phases of the cell cycle were abnormal. However, specific measurements of the duration of the cell cycle in different phases are needed to confirm this.

BAF complexes have been shown to participate in different aspects of the cell cycle both as promoters and inhibitors of cell proliferation. In particular, Smarce1 has been shown to promote cell proliferation in HeLa cells as part of the pBAF complex (Hah et al., 2010). As previously mentioned, inactivation of the BAF ATPase subunit Smarca4 in zebrafish is described as the *young* mutation (Link et al., 2000; Gregg et al., 2003). *Young* mutant fish present severe defects in retinogenesis. Many of these defects are shared by *smarce1*-mutants and are discussed below. With respect to proliferation, in a study by Link *et al.*, analysis of BrdU incorporation indicated that in *young* mutants, the initiation and pattern of cell cycle withdrawal across the retina was normal, suggesting no deficiency in proliferation. However, they did not evaluate mitosis and did not consider the same developmental stages; therefore, we cannot fully compare the cell cycle phenotypes of the *young* and *smarce1* mutants. Thus, whether Smarca4 and Smarce1 play the same role in RPCs proliferation is not clear. However, in mice, clonal expansion of Smarca4-deficient retinal progenitors is reduced, and cell cycle progression is delayed (Aldiri et al., 2015). Thus, the mouse *Smarca4*-mutant phenotype would be more similar to that of the zebrafish *smarce1* mutant in this respect. It is important to define the subunit composition of the active BAF complex in retinal progenitors to determine whether it incorporates the Brg1 or the Brm subunit, as this information may help to elucidate the phenotypic differences in the cell cycle between the *young* and the *smarce1* mutants.

Another factor that contributes to microphthalmia is cell death, which was elevated in the *smarce1*-mutants together with an increased expression of apoptosis-related genes. At 5 dpf, we detected holes of significant size in DAPI stained single-sections, which suggested that cell death might be the major cause of the reduction in the eye size (Supplementary Fig2). Additionally, we hypothesize that this cell death triggers an immune response, which would explain the upregulation of pathways implicated in inflammation and the immune response. It is interesting that immune response-related genes are also overexpressed in the retinas of Smarca4 conditional mutant mice, where cell death has also been reported. On the other hand, in the *young*-mutant zebrafish, no cell death experiments were performed.

Among the phenotypes that are shared by both zebrafish and mouse Smarca4-mutants and the zebrafish *smarce1*-mutant is the defective retinal lamination including the alterations of plexiform layers and the mislocalization of differentiated neurons. Additionally, in the three mutants, the determination of the cell fate of all the neuronal types was normal. We did not identify the mechanisms underlying the disorganization of the retinal layers in the *smarce1*-mutant. Proper organization of the retinal layers requires the production of different neuronal types in the correct proportions at precise developmental stages; thus, the laminar defects could be a secondary effect of the cell cycle abnormalities. However, neuronal lamination is a complex process that, in addition to the generation of the right types and number of cells, depends on very carefully coordinated cell translocation events in order to position neurons in the correct locations. All these movements involve diverse interactions both between cells and the extracellular matrix. Molecules involved in this process include β-catenin, N-cadherin, F-actin, laminins, and polarity-related genes (Amini et al., 2017). According to our transcriptomic profile, none of these pathways were significantly affected at

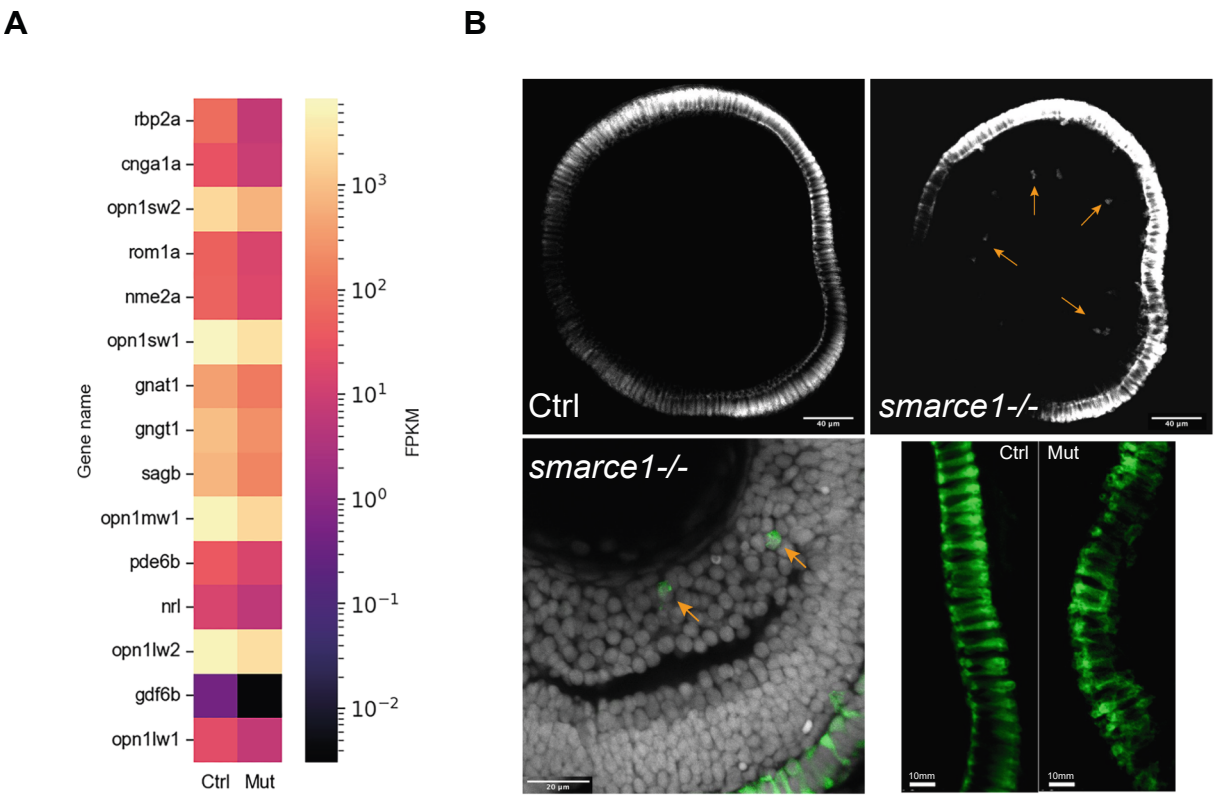

Fig. 6. Terminal differentiation of PRs is defective. (A) Heatmap showing the top downregulated genes of the Phototransduction Term. The bar shows the average FPKM value of three replicates. Yellow color indicates a high expression level, and black color indicates a low expression level. Genes are organized according to their Padj value from small to large (range 3.8–64 to 0.00749). (B) Confocal sections of 5 dpf Ctrl and *smarce1*$^{-/-}$ retinas stained with the Zpr1 antibody (green). Ectopic cones are visible in inner locations (yellow arrows) in the mutant images. Right lower panel shows a closer caption of the PRs where disorganization can be appreciated. Scale bars, upper panel:40 µm; left lower panel: 20 µm; right lower panel: 10 µm. (For interpretation of the references to colour in this figure legend, the reader is referred to the web version of this article.)

the transcript level. It remains to be determined whether their functions are normal. In *young* mutant fish, mosaic analysis revealed that defective lamination was due to nonautonomous effects (Link et al., 2000); therefore, this might be the case for the *smarce1*-mutation.

Based on the results of the DEG analysis, we believe that the differentiation of most cell types was not affected because genes associated with terminal differentiation were not differentially expressed. The only cells whose differentiation is altered were the PRs, as indicated by the phototransduction pathway, which was strongly dysregulated (Fig. 6A). This result is in line with the expression of Smarce1 in PRs and its absence in other neuronal types. We propose that in these cells Smarce1 plays an intrinsic role in these cells. This finding coincides with what was found in *Brg1* mutant mice and diverges from what was found in the *young* mutant. An intriguing finding is the detection of a strong signal of Smarce1 in a significant number of ACs, as we did not observe any remarkable phenotypical change in this neuronal type. Clearly, not all subtypes of amacrine cells express Smarce1, for example, those that reside in the ganglion cell layer are negative. At 5 dpf 28 distinct amacrine subtypes are present in the retina (Jusuf and Harris, 2009); thus, specific identification of subtypes is needed to eliminate the possibility that some subtypes are reduced or expanded at the expense of others. With respect to differential expression, we did not find altered expression of genes that characterize terminal differentiation of amacrine cells, such as *calretinin, parvalbumin, sox2, GABA* or *glycine*. The only genes that presented a significant change in expression were *ptf1a,* which was downregulated, and the horizontal cell markers *onecutl* and *onecut2*, which were upregulated. Another relevant information worth to be considered is that the *smarce1* gene can contribute to the diversity of the BAF complexes, at least in humans and rodents, where N-terminal deletions (N-BAF57) preceding the HMG domain are produced by alternative splicing and expressed specifically in the brain (Kazantseva et al., 2009). PCR analysis of the zebrafish transcripts indicated that homologous exons can also be alternatively spliced in zebrafish. In our CRISPR-Cas9 mutant, these exons were not targeted by the RNA guide; therefore, the spliced isoforms would still be functional in our *smarce1*-mutant. Thus, it is likely that the phenotypes that we observe, in general and particularly in the amacrine cells, are partially rescued by the remaining isoforms. It would be interesting to target all isoforms of Smarce1 in a future experiment.

In conclusion, in this work, we followed the development of the retina in zebrafish with a mutation in the *smarce1* gene, a critical subunit of the BAF complex. We showed that Smarce1 is required to maintain late retinal progenitor cell proliferation and for the correct organization of the retinal layers. The loss of Smarce1 provokes intensive cell death and retinal degeneration, which together lead to the activation of different forms of the immune response. Not all of these phenotypes are shared by the *brg1*-mutant zebrafish, which suggests that a differential configuration of the BAF complex in the retina contributes to distinct functions during retinogenesis. The most conserved phenotypes associated with the loss of the BAF complex in fish and mice were the microphthalmia and defective laminar organization, which were also observed in the previously mentioned study by Gregg *et al* (Gregg et al., 2003), that includes a preliminary analysis of a mutation in *baf53*, which encodes a subunit that also complexes with Brg1. No other subunits of the BAF complex have been studied in the context of retina formation. A detailed analysis of the organization of the BAF subcomplexes in the retina and strategic mutagenesis of specific subunits would be useful to understand the precise cell type- and developmental stage-specific

activities of the SWI-SNF remodeler during eye development.

CRediT authorship contribution statement

Laura Ramírez: Writing – review & editing, Investigation, Data curation. **Denhí Schnabel:** Writing – review & editing, Investigation. **Flavio R. Zolessi:** Writing – review & editing, Supervision, Methodology, Formal analysis, Data curation. **Hilda Lomelí:** Writing – review & editing, Writing – original draft, Supervision, Investigation, Funding acquisition, Formal analysis, Data curation, Conceptualization.

Funding

This work was supported by DGAPA-UNAM grant IN206822.

Declaration of Competing Interest

The authors declare that they have no known competing financial interests or personal relationships that could have appeared to influence the work reported in this paper.

Acknowledgments

We thank Jaime Carlos López Rodríguez for assistance with bioinformatic analysis; Jaime Arturo Pimentel Cabrera and Julio César Valerio Negreros for technical assistance in confocal microscopy; Dulce Pacheco for help with fish maintenance, and the librarian Shirley Ainsworth for her technical support.

Appendix A. Supplementary data

Supplementary data to this article can be found online at https://doi.org/10.1016/j.neuroscience.2025.09.045.

References

Aigner, S., Denli, A.M., Gage, F.H., 2007. A novel model for an older remodeler: the BAF swap in neurogenesis. Neuron 55, 171–173.

Aldiri, I., Ajioka, I., Xu, B., Zhang, J., Chen, X., Benavente, C., Finkelstein, D., Johnson, D., Akiyama, J., Pennacchio, L.A., Dyer, M.A., 2015. Brg1 coordinates multiple processes during retinogenesis and is a tumor suppressor in retinoblastoma. Development 142, 4092–4106. https://www.ncbi.nlm.nih.gov/pubmed/26628093.

Almeida, A.D., Boije, H., Chow, R.W., He, J., Tham, J., Suzuki, S.C., Harris, W.A., 2014. Spectrum of Fates: a new approach to the study of the developing zebrafish retina. Development 141, 1971–1980. https://www.ncbi.nlm.nih.gov/pubmed/24718991.

Amini, R., Rocha-Martins, M., Norden, C., 2017. Neuronal Migration and Lamination in the Vertebrate Retina. Front. Neurosci. 11, 742. https://www.ncbi.nlm.nih.gov/pubmed/29375289.

Bernardos, R.L., Raymond, P.A., 2006. GFAP transgenic zebrafish. Gene Expr. Patterns 6, 1007–1013. https://www.ncbi.nlm.nih.gov/pubmed/16765104.

Cardiff, R.D., Miller, C.H., Munn, R.J., 2014. Manual hematoxylin and eosin staining of mouse tissue sections. Cold Spring Harb Protoc 2014, 655–658. https://www.ncbi.nlm.nih.gov/pubmed/24890205.

Castillo-Robles, J., Ramírez, L., Spaink, H.P., Lomelí, H., 2018. smarce1 mutants have a defective endocardium and an increased expression of cardiac transcription factors in zebrafish. Sci. Rep. 8, 15369. https://www.ncbi.nlm.nih.gov/pubmed/30337622.

Gourisankar, S., Krokhotin, A., Wenderski, W., Crabtree, G.R., 2024. Context-specific functions of chromatin remodellers in development and disease. Nat. Rev. Genet. 25, 340–361. https://www.ncbi.nlm.nih.gov/pubmed/38001317.

Gregg, R.G., Willer, G.B., Fadool, J.M., Dowling, J.E., Link, B.A., 2003. Positional cloning of the young mutation identifies an essential role for the Brahma chromatin remodeling complex in mediating retinal cell differentiation. PNAS 100, 6535–6540.

Gregg, R., Willer, G., Fadool, J., Dowling, J., Link, B., 2003. Positional cloning of the young mutation identifies an essential role for the Brahma chromatin remodeling complex in mediating retinal cell differentiation. PNAS 100, 6535–6540.

Hah, N., Kolkman, A., Ruhl, D.D., Pijnappel, W., Heck, A.J.R., Timmers, H.T.M., Kraus, W.L., 2010. A Role for BAF57 in cell cycle-dependent transcriptional regulation by the SWI/SNF chromatin remodeling complex. Cancer Res. 70, 4402–4411.

Hodges, C., Kirkland, J., Crabtree, G., 2016. The many roles of BAF (mSWI/SNF) and PBAF complexes in cancer. Cold Spring Harb. Perspect. Med. 6.

Iida, A., Iwagawa, T., Baba, Y., Satoh, S., Mochizuki, Y., Nakauchi, H., Furukawa, T., Koseki, H., Murakami, A., Watanabe, S., 2015. Roles of histone H3K27 trimethylase Ezh2 in retinal proliferation and differentiation. Dev. Neurobiol. 75, 947–960. https://www.ncbi.nlm.nih.gov/pubmed/25556712.

Jusuf, P.R., Harris, W.A., 2009. Ptf1a is expressed transiently in all types of amacrine cells in the embryonic zebrafish retina. Neural Dev. 4, 34. https://www.ncbi.nlm.nih.gov/pubmed/19732413.

Kadoch, C., Crabtree, G., 2015. Mammalian SWI/SNF chromatin remodeling complexes and cancer: Mechanistic insights gained from human genomics. Sci. Adv. 1.

Kazantseva, A., Sepp, M., Kazantseva, J., Sadam, H., Pruunsild, P., Timmusk, T., Neuman, T., Palm, K., 2009. N-terminally truncated BAF57 isoforms contribute to the diversity of SWI/SNF complexes in neurons. J. Neurochem. 109, 807–818.

Kimmel, C.B., Ballard, W.W., Kimmel, S.R., Ullmann, B., Schilling, T.F., 1995. Stages of embryonic development of the zebrafish. Dev. Dyn. 203, 253–310. https://www.ncbi.nlm.nih.gov/pubmed/8589427.

Larison, K.D., Bremiller, R., 1990. Early onset of phenotype and cell patterning in the embryonic zebrafish retina. Development 109, 567–576. https://www.ncbi.nlm.nih.gov/pubmed/2401210.

Lessard, J., Wu, J.I., Ranish, J.A., Wan, M., Winslow, M.M., Staahl, B.T., Wu, H., Aebersold, R., Graef, I.A., Crabtree, G.R., 2007. An essential switch in subunit composition of a chromatin remodeling complex during neural development. Neuron 55, 201–215. https://www.ncbi.nlm.nih.gov/pubmed/17640523.

Letelier, J., Buono, L., Almuedo-Castillo, M., Zang, J., Mounieres, C., González-Díaz, S., Polvillo, R., Sanabria-Reinoso, E., Corbacho, J., Sousa-Ortega, A., Diez Del Corral, R., Neuhauss, S.C.F., Martínez-Morales, J.R., 2023. Mutation of. Elife 12. https://www.ncbi.nlm.nih.gov/pubmed/37227126.

Link, B.A., Fadool, J.M., Malicki, J., Dowling, J.E., 2000. The zebrafish young mutation acts non-cell-autonomously to uncouple differentiation from specification for all retinal cells. Development 127, 2177–2188. https://www.ncbi.nlm.nih.gov/pubmed/10769241.

Lomeli, H., Castillo-Robles, J., 2016. The developmental and pathogenic roles of BAF57, a special subunit of the BAF chromatin-remodeling complex. FEBS Lett. 590, 1555–1569.

Malicki, J., Pooranachandran, N., Nikolaev, A., Fang, X., Avanesov, A., 2016. Analysis of the retina in the zebrafish model. Methods Cell Biol. 134, 257–334. https://www.ncbi.nlm.nih.gov/pubmed/27312496.

Mashtalir, N., D'Avino, A.R., Michel, B.C., Luo, J., Pan, J., Otto, J.E., Zullow, H.J., McKenzie, Z.M., Kubiak, R.L., St Pierre, R., Valencia, A.M., Poynter, S.J., Cassel, S. H., Ranish, J.A., Kadoch, C., 2018. Modular organization and assembly of SWI/SNF family chromatin remodeling complexes, 1272–1288.e1220 Cell 175. https://www.ncbi.nlm.nih.gov/pubmed/30343899.

Mendieta-Serrano, M.A., Mendez-Cruz, F.J., Antúnez-Mojica, M., Schnabel, D., Alvarez, L., Cárdenas, L., Lomelí, H., Ruiz-Santiesteban, J.A., Salas-Vidal, E., 2019. NADPH-Oxidase-derived reactive oxygen species are required for cytoskeletal organization, proper localization of E-cadherin and cell motility during zebrafish epiboly. Free Radic. Biol. Med. 130, 82–98. https://www.ncbi.nlm.nih.gov/pubmed/30342187.

Niklaus, S., Neuhauss, S.C.F., 2017. Genetic approaches to retinal research in zebrafish. J. Neurogenet. 31, 70–87. https://www.ncbi.nlm.nih.gov/pubmed/28678567.

Norden, C., 2023. A fish eye view: retinal morphogenesis from optic cup to neuronal lamination. Annu. Rev. Cell Dev. Biol. 39, 175–196. https://www.ncbi.nlm.nih.gov/pubmed/37418775.

Prieto, D., Aparicio, G., Machado, M., Zolessi, F.R., 2015. Application of the DNA-specific stain methyl green in the fluorescent labeling of embryos. J. Vis. Exp., e52769. https://www.ncbi.nlm.nih.gov/pubmed/25993383.

Qi, J., Dong, Z., Shi, Y., Wang, X., Qin, Y., Wang, Y., Liu, D., 2016. NgAgo-based fabp11a gene knockdown causes eye developmental defects in zebrafish. Cell Res. 26, 1349–1352. https://www.ncbi.nlm.nih.gov/pubmed/27834346.

Raeisossadati, R., Ferrari, M.F.R., Kihara, A.H., AlDiri, I., Gross, J.M., 2021. Epigenetic regulation of retinal development. Epigenetics Chromatin 14, 11. https://www.ncbi.nlm.nih.gov/pubmed/33563331.

Stenkamp, D.L., 2015. Development of the Vertebrate Eye and Retina. Prog. Mol. Biol. Transl. Sci. 134, 397–414. https://www.ncbi.nlm.nih.gov/pubmed/26310167.

Xu, B., Tang, X., Jin, M., Zhang, H., Du, L., Yu, S., He, J., 2020. Unifying developmental programs for embryonic and postembryonic neurogenesis in the zebrafish retina. Development 147. https://www.ncbi.nlm.nih.gov/pubmed/32467236.

Yin, W., Mao, X., Xu, M., Chen, M., Xue, M., Su, N., Yuan, S., Liu, Q., 2023. Epigenetic regulation in the commitment of progenitor cells during retinal development and regeneration. Differentiation 132, 51–58. https://www.ncbi.nlm.nih.gov/pubmed/37069005.

Zhang, J., Taylor, R.J., La Torre, A., Wilken, M.S., Cox, K.E., Reh, T.A., Vetter, M.L., 2015. Ezh2 maintains retinal progenitor proliferation, transcriptional integrity, and the timing of late differentiation. Dev. Biol. 403, 128–138. https://www.ncbi.nlm.nih.gov/pubmed/25989023.

Zhu, Z., Chen, X., Guo, A., Manzano, T., Walsh, P.J., Wills, K.M., Halliburton, R., Radko-Juettner, S., Carter, R.D., Partridge, J.F., Green, D.R., Zhang, J., Roberts, C.W.M., 2023. Mitotic bookmarking by SWI/SNF subunits. Nature 618, 180–187. https://www.ncbi.nlm.nih.gov/pubmed/37225980.

Zolessi, F.R., Poggi, L., Wilkinson, C.J., Chien, C.B., Harris, W.A., 2006. Polarization and orientation of retinal ganglion cells in vivo. Neural Dev. 1, 2. https://www.ncbi.nlm.nih.gov/pubmed/17147778.